Available online at www.sciencedirect.com

ScienceDirect

Energy Procedia 98 (2016) 115 – 124

Energy Procedia

6th Workshop on Metallization and Interconnection for Crystalline Silicon Solar Cells, 2016

Materials challenge for shingled cells interconnection

Guy Beaucarne*

Dow Corning Europe S.A., Parc Industriel, Zone C, Rue Jules Bordet, 7180 Seneffe, Belgium

Abstract

This paper discusses some challenges that need to be tackled when designing a photovoltaic module using a shingled cells structure. We derive a simple analytical model to determine the conditions needed to avoid interconnection joint failure. It is found that interconnection materials with a low ratio of shear modulus G over shear strength $\tau_{sh.\ str.}$ is preferred for good interconnection joints reliability. As a result, solder joints appear inappropriate for the application, while electrically conductive adhesives (ECA) with low G/ $\tau_{sh.\ str}$ can better fulfill the requirements. An interconnection approach is also proposed which makes use of a combination of adjacent ECA and a non-conductive adhesive materials in a shingled configuration to help achieve string robustness and reliability.

Peer-review under responsibility of the organizing committee of the Metallization Workshop 2016

Keywords: Interconnection ; electrically conductive adhesive ; shingled cells

1. Introduction

The traditional technique to interconnect solar cells in a module is to solder Cu ribbons onto Ag busbars present on the front and the rear of solar cells. This approach has proved to be cheap and, if the soldering process, stringing process and ribbon parameters are well designed and controlled, it is robust and reliable. However, there are several problems associated with this technology. First, the ribbons and front busbars cause substantial shading losses. Moreover, the busbars cover a significant area of the solar cells and are made of almost pure Ag, which is an important cost. Further, as the large cell current is forced into ribbons with a small cross-section, resistive losses are high. Another limitation of ribbon soldering is the differential contraction of the copper ribbons and the silicon,

* Corresponding author. Tel.: +32-64-889-294; fax: +32-64-888-950
E-mail address: guy.beaucarne@dowcorning.com

Peer-review under responsibility of the organizing committee of the Metallization Workshop 2016
doi:10.1016/j.egypro.2016.10.087

which can result in high stress in the metallization and silicon. Moreover soldering local heating and pressure and can contribute to additional stress and micro-cracks in the silicon. As a result soldering interconnection prevents the evolution towards thinner wafers because stress-related yield losses soar when going thinner. Finally, the types of solder materials that are mostly used contain a large amount of Pb, which causes a regulatory concern for the future.

Several new module concepts, which make use of new interconnection technologies and new cell types, are presently being developed and introduced in the market, for instance multiwire interconnection on busbarless cells and conductive backsheet interconnection with back-contact cells. In this paper, we discuss one of these concepts, namely the shingled cells module.

2. Shingled cells module structure

In the shingled cells module structure, the cells that are used are rectangular (Fig.1). The long side usually has the length corresponding the side length of a standard solar wafer, i.e. 15.6 cm. The short side is only a few cm long. Usually, these solar cell strips have been cut out from a processed device with standard size 15.6 x 15.6 cm^2. The cells have busbars or rows of solder pads along the long edge, one on the front and one on the back (opposite edge).

a)

b)

Fig. 1. Schematic drawing of a cell for shingled cells interconnection. (a) top view ; (b) bottom view

To create a cells string, an interconnection material is applied to connect the rear busbar of a cell with the front busbar of the next cell (Fig. 2). The cells overlap each other slightly, so that the front busbars are covered by the edge region of the adjacent cell, just like shingles on a roof (Fig. 3). Because there is no spacing between cells as in conventional modules, because the cell area that is shaded by the front busbar is covered by an active area of another cell, and as there is no ribbon covering the cells' front surface and causing shading, this structure results into modules with extremely high active area to total area ratio, allowing in principle very high module efficiency. One also saves on ribbon cost, but there is the extra cost of cutting the cells into strips. The cell cutting process may cause some cracks and related failures and therefore needs to be well-controlled.

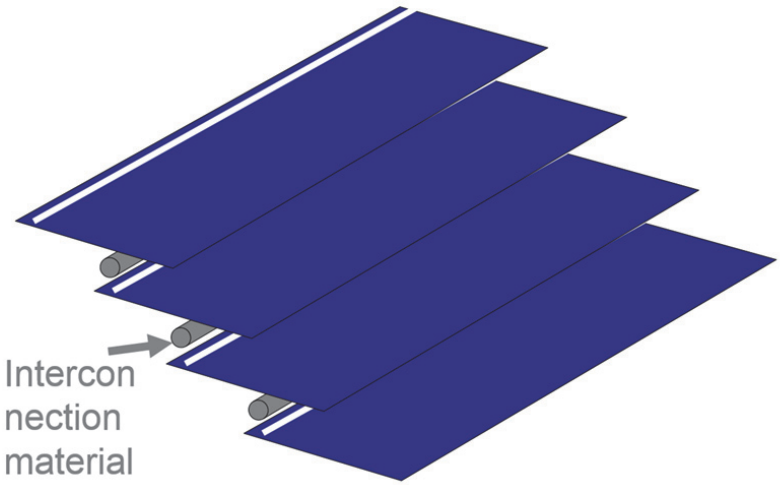

Fig. 2. Schematic drawing of the cells shingling principle

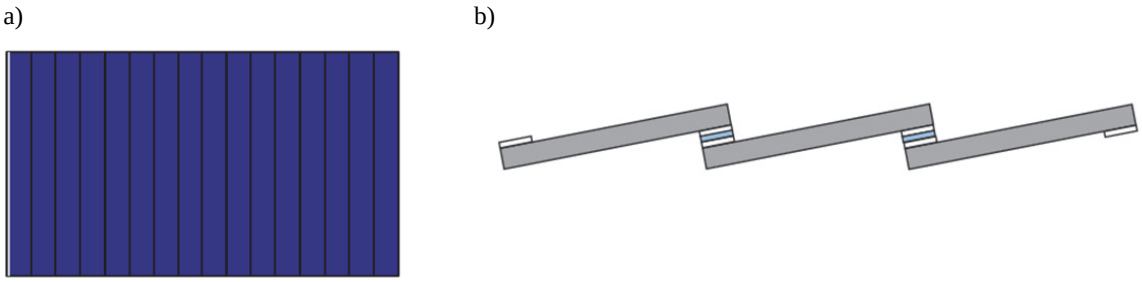

Fig. 3. Schematic drawing of a shingled cells string : a) top view ; b) cross-section. Note that in the drawing, for clarity, the y-direction is very much expanded compared to the x-direction. In reality the cells lie almost flat in a module.

Solar cells shingling is not new. In the early days of photovoltaics, such structures were developed for space modules (e.g. [1]). Later on, in the 1990's, high efficiency shingled cells modules were made for use in race solar cars [2-4]. Recently, there has been a new surge of interest for this type of modules. First, technological start-ups started developing modules based on shingling [5], [6], [7]. Subsequently, those technologies were acquired or licensed and are being further developed and commercialized by large PV companies [8], [9].

3. Analytical model

3.1. Preliminary considerations

Because photovoltaic modules consist of several different materials, which all have their own coefficient of thermal expansion, it is expected that, as temperature varies, there will be some relative movement between components within the module, which will induce mechanical stress if constrained. We have the same situation in standard modules with soldered ribbons interconnection. However, traditional interconnection, featuring several mm between the cells and Cu ribbons that can easily bend, is quite forgiving in terms of relative movement. This is

illustrated in Fig. 4. If the thermomechanical situation is such that two cells are pushed towards each other, the ribbon will deform slightly to allow the movement. The encapsulant is generally soft in comparison with the other materials and will also allow the movement. With shingled interconnection, the cells movement is much more constrained and the joints between the cells have to allow some movement by deformation while bearing some stress.

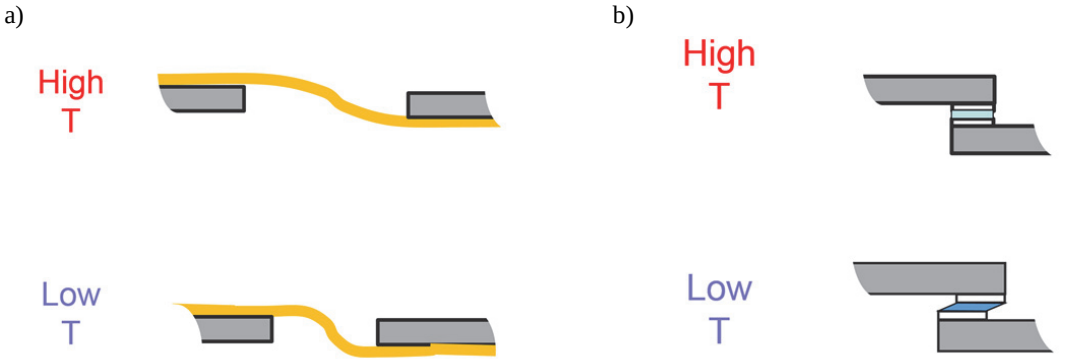

Fig. 4. Schematic illustration of thermomechanical difference between traditional interconnection and shingled cells interconnection: a) deformation of copper ribbon allows relative cell movement ; b) Interconnection in shingled structure requires some deformation of joint material and shear stress bearing capability

A full study of stress during thermal cycling would require numerical finite elements thermomechanical modelling of a complete module, which is beyond the scope of this paper. Here, we just establish a simple analytical model to identify the parameters that are important for internal stress.

3.2. Model

Fig. 5 shows the shingled strings structure that we aim to model in cross-section. There are n cells and therefore n-1 joints.

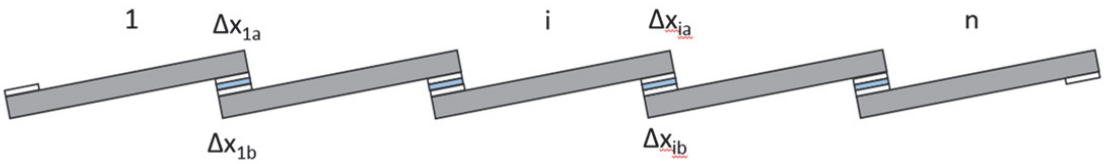

Fig. 5. Modelled shingled cells structure

Although the y direction has been expanded in the drawing for clarity, the structure is in reality much flatter, and cells and joints are essentially horizontal. For simplicity, it is assumed that the overlap region corresponds to the joint width. The right end of the i^{th} cell has a position $x_{ia}(T_0)$ at the reference temperature. When temperature change, that point will move to $x_{ia}(T)$. The change in position is Δx_{ia}. The left end of the $i+1^{th}$ cell will also move and result in a change in position Δx_{ib}, but these changes will not necessarily be equal. The difference will give a relative displacement which causes strain and stress in the joint (Fig. 6). In our model, we determine this relative displacement and use it to derive strain and stress in the joint.

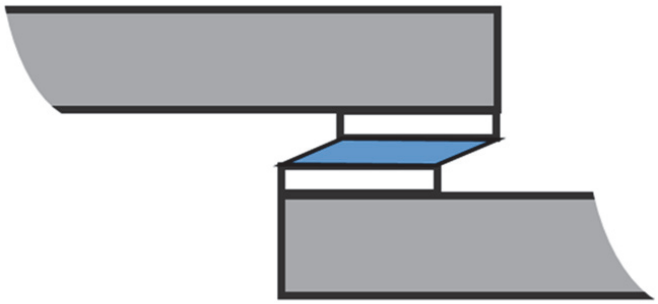

Fig. 6. Interconnection joint under strain in shingled cells structure

Let us assume that the joints were formed at high temperature, e.g. 150 °C. At that temperature, there is no stress in the structure. When the string is unrestrained and cooled down to say – 50 °C, the silicon cells will shrink and the whole string will become shorter. Because it is unrestrained, the movement will not be opposed, and no stress will be created. In a module however, the strings are restrained because the components are mechanically bonded to each other. Now, we make a first main assumption. We assume the glass panel dominates the thermomechanical behavior of the assembly as a whole, as it is by far the largest and thickest component, and one of the stiffest. This assumption seems justified based on experimental measurements of component displacement when modules are cooled down in climate chambers [10] , [11].

Making that assumption, we conclude that the total deformation of the string in the x direction will be equal to the deformation of the glass panel above it.

$$\Delta L = L_0 \alpha_{glass} \Delta T \quad (1)$$

Here, L_0 is the length of the cells string (and of the part of the glass panel covering the string) at the stress-free temperature, α_{glass} is the Coefficient of Thermal Expansion (CTE) of glass, and ΔT is the difference in temperature between the temperature considered and the stress-free temperature. Since silicon has a lower CTE than glass, it is going to shrink less. As a result some stress will build up, and that shear strain will appear at the joints.

In order to continue the discussion analytically, we make the simplifying assumption that there is no shear force working on the string, and that the string is constrained by two longitudinal forces, equal but opposite and applied on the first and last cell. We will see later that this leads to underestimation of the maximum joint stress, but it is a useful case to get order of magnitude values and gain insight in the important factors.

Basic statics tells us that the two joints on each cell are applying equal but opposite shear forces on the cell (Fig.7), and that those forces are the same for all cells. To be totally correct, one should mention a force couple present in the joint region and which ensures that there is no rotation. However, those forces are comparatively small and do not change anything to the reasoning and outcome of the model.

Fig. 7. Situation of forces applied to a cell in the string in the simplified model

Shear forces are correspondingly applied by cells on each joint

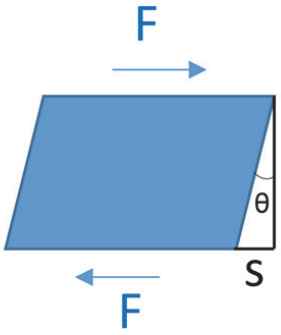

Fig. 8. Situation of forces applied to an interconnection joint in the simplified model

Now we introduce another assumption: we assume that all the strain in the string is occurring in the joints and not in the silicon. This is reasonable as long as the Young's modulus of the joint material is much lower than that of silicon, which is true for all relevant potential joint materials. Additionally, we assume that the cells do not bend and that the cells string does not buckle, that is deforming by going out of plane.

Hooke's law states that :

$$\tau = G\gamma \tag{2}$$

with τ the shear stress in the joint, G the shear elasticity modulus of the joint material, and γ the shear strain. Note that we assume that we have a situation with only shear strain and shear stress.

Trigonometry tells us that (see Fig.8) :

$$\tan\theta = \frac{s}{t} \tag{3}$$

with s the relative lateral shift of the two joint surfaces caused by the strain, t the joint thickness and θ the angle between the edge of the joint and the normal.

Now, θ is equal to the shear strain γ. Moreover, θ is small, so $\tan\theta \approx \theta$. As a result,

$$\tau = G\theta = G\tan\theta = \frac{Gs}{t} \tag{4}$$

The total length of the string at a given temperature can be expressed as

$$nl - (n-1)w - (n-1)s \tag{5}$$

with l the cell length in the longitudinal direction and w width of the overlap region (equal to the joint width).

The difference between the total length at the stress-free temperature and the length at a given temperature is given by

$$nl_0\alpha_{Si}\Delta T - (n-1)w_0\alpha_{Si}\Delta T - (n-1)s \tag{6}$$

or :

$$\alpha_{Si}\Delta T[nl_0 - (n-1)w_0] - (n-1)s \tag{7}$$

Equating the total deformation of the string in the x direction to the deformation of the glass above it (equation (1)) gives :

$$L_0\alpha_{glass}\Delta T = \alpha_{Si}\Delta T[nl_0 - (n-1)w_0] - (n-1)s$$

Isolating s, we find :

$$s = \frac{-\Delta T\{L_0\alpha_{glass} - \alpha_{Si}[nl_0 - (n-1)w_0]\}}{(n-1)} \tag{8}$$

We fill that expression in (4) and find

$$\tau = \frac{G(-\Delta T)\{L_0\alpha_{glass} - \alpha_{Si}[nl_0 - (n-1)w_0]\}}{t(n-1)} \tag{9}$$

The joint will fail when shear stress τ will reach or exceed the material shear strength $\tau_{sh.\ str.}$, so when

$$\frac{G(-\Delta T)\{L_0\alpha_{glass} - \alpha_{Si}[nl_0 - (n-1)w_0]\}}{t(n-1)} \geq \tau_{sh.\ str.} \tag{10}$$

So the condition one should maintain to avoid joint failure is

$$\frac{G(-\Delta T)\{L_0\alpha_{glass} - \alpha_{Si}[nl_0 - (n-1)w_0]\}}{\tau_{sh.\ str.}\ t(n-1)} < 1 \tag{11}$$

We now come back to the assumption of no external shear force on the string. Assume that there is locally an external shear force (for instance applied by the encapsulant on the string). In any case, the total string deformation is the same, since it is determined by the shrinkage of the glass panel. If an additional shear force is working in a region of the string, causing a higher string compression, which will cause a higher stress in the joints than in the no external shear force case. It will be compensated by regions of the string where there is less string compression than in the no external shear force case. The shear stress expression in (9) therefore provides a lower bound for the

maximum shear stress occurring in a joint at a given temperature differential compared to the stress-free temperature.

Another remark that needs to be made regarding this equation is that it assumes that failure will always occur cohesively. So implicitly, we assume that the joint material has an excellent adhesion to the busbars. If the joint material shows some adhesive failure on the busbar material, another expression than (11) is required to adequately describe the conditions under which failure will not occur.

4. Discussion

It is clear that the left hand side of (11) should be minimized to avoid joint failure. Some parameters are fixed and cannot be changed either by module design of joint material selection. The CTE of glass, or the maximum temperature differential are fixed by material properties or application demands that cannot be changed. However, the design and the nature of the joint material are parameters than can be chosen.

4.1. Design aspects

For a given L_0, equation (11) tells us that it is better to have a high n, which means that many small cells connected with many joints is better than longer cells with fewer joints. This is because there are more places where relative displacement is allowed. However, in practice, the length of the cells is dictated by practical and economic considerations (smaller cells implies more cutting, more complicated handling and higher edge losses).

Another design parameter than can be varied is joint thickness t. By choosing a thicker joint, the maximum stress is decreased and the probability of failure occurrence is decreased. Here again, there may be practical and economical aspects that limit freedom when selecting joint thickness (for instance material cost considerations).

4.2. Material aspects

The joint material turns out to be critical. There are two joint material parameters in (11) : G the shear modulus and $\tau_{sh.\ str.}$, the shear strength. Equation (11) tells us that the ratio $G/\tau_{sh.\ str}$ should preferably be as low as possible to minimize the chances of joint failure. Therefore this ratio should be taken in consideration when selecting the joint material. Table 1 lists different material types that can be considered for this application, a SnPb solder alloy and two types of electrically conductive adhesives (ECA). The table gives ranges of values for G, $\tau_{sh.\ str}$, and $G/\tau_{sh.\ str}$. It should be mentioned that the ranges correspond to the lowest and highest values that the author found in the literature and technical information documents. There may be other materials within each material types that have values outside those ranges. Nevertheless general statements can be made.

Table 1. Parameters of some potential materials to be used in interconnection joints in shingled cell modules

	Eutectic tin lead solder	Epoxy ECA	Silicone ECA
G (MPa)	11000 - 14000	200 - 2000	10 - 100
$\tau_{sh.\ str.}$ (MPa)	23 - 48	5 - 10	0.3 - 1
$G/\tau_{sh.\ str}$	230 - 600	20 - 400	10 - 300
Resistivity (ohm cm)	0.15×10^{-4}	$1 – 25 \times 10^{-4}$	$2 – 30 \times 10^{-4}$

Tin lead solder alloy is very stiff, and the ratio $G/\tau_{sh.\ str}$. is very high. That material therefore appears unsuitable for the application. It should be noted that the depicted situation is too simple for the reality of solder mechanical behavior. In reality, solder undergoes plastic deformation well before it fails cohesively. That plastic deformation relieves some of the stress. However, repeated occurrence of plastic deformation may ultimately lead to failure. An analysis of this phenomenon in shingled cells modules is beyond the scope of this paper.

Epoxy-based ECA tend to be rather stiff but show a high shear strength. Silicone ECAs on the other hand are much more flexible (very low G) but usually have lower shear strength. Depending on the composition of a particular ECA, the G/ $\tau_{sh.\ str}$. of that ECA ratio maybe low or high. ECAs can be engineered to achieve a good compromise between the key different properties (shear strength, elasticity modulus and resistivity). This formulation flexibility is an advantage for ECAs.

Silicone ECAs are attractive in this application, not only because of the relatively low G at room temperature, but also because the mechanical properties vary little over the whole operating temperature range of PV modules [12],[13]. Organic ECAs in contrast go through their glass transition temperature within that range and are in their glassy, brittle state at strongly negative temperatures (- 10 °C and below). This even applies to those epoxy ECAs that have been engineered for a reduced Tg (around 0 °C).

It should be noted that the present study only dealt with thermal mismatch-induced stress, which is a static load. If one starts adding weight, module bending and dynamic loads, stress in the interconnection will be modified. It will depend on the module structure (for instance, a double glass module typically will fare better than a glass-backsheet module), but generally, it can be expected that stress and risk of failure will increase.

4.3. Two materials solution

ECAs are highly filled materials, typically more than 70 w% and often higher than 80 w% conductive filler particles. This is needed to ensure multiple percolation paths and provide good electrical conductivity and low contact resistance. Conductive filler particles however typically do not provide reinforcing properties and do not contribute to material cohesion. As a result, ECAs' intrinsic mechanical strength is much poorer than the same materials without filler. In order to obtain an interconnection that gives both good electrical contact and mechanically strong bond, we suggest combining an ECA with a much stronger non-conductive adhesive. These materials could be a silicone ECA and a non-conductive, flexible but strong silicone adhesive. Effectively, this creates a hybrid material with adequate conductivity and lower G/ $\tau_{sh.\ str}$ ratio, which would enhance interconnection robustness particularly in extreme conditions. Although the drawing shows alternating dots of ECA and NCA, other configurations could be implemented, such two parallel lines.

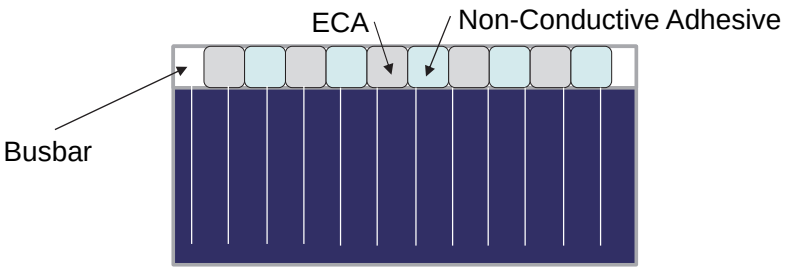

Fig. 9. Suggested 'hybrid' interconnection structure combining ECA and non-conductive adhesive

5. Conclusion

We discussed the shingled cells interconnection concept and presented a simplified analytical model for the thermomechanics of such structures. It is found that interconnection materials with a low ratio of shear modulus G over shear strength $\tau_{sh.\ str.}$ is preferred for good interconnection joints reliability. As a result, solder joints appear inappropriate for the application, while electrically conductive adhesives (ECA) with low G/ $\tau_{sh.\ Str.}$ can better fulfill the requirements. An interconnection approach is also proposed which makes use of a combination of adjacent

ECA and a non-conductive adhesive materials in a shingled configuration to help achieve string robustness and reliability even in extreme conditions .

References

[1] Patent US3369939A, J.H. Myer, 1962
[2] J. Zhao, A.Wang, F. Yun, G. Zhang, D. M. Roche, S. R. Wenham and M. A. Green, 20 000 PERL Silicon Cells for the `1996 World Solar Challenge' Solar Car Race, Progress in Photovoltaics 5(1997).
[3] Patent DE3942205A1, J.S. H. Gochermann, 1989
[4] M. A. Green, K.Emery, Y. Hishikawa, W. Warta, E. D. Dunlop, Solar cell efficiency tables (version 46), Progress in Photovoltaics, 23 (2015) 805-812.
[5] 'Cogenra Wins $2M U.S. Energy Dept. SunShot Award ' in Business wire, 2014, http://www.businesswire.com/news/home/20141022006260/en/Cogenra-Wins-2M-U.S.-Energy-Dept.-SunShot#.VJByRCvF9W-
[6] Webpage 'Technical datasheet PowerXT™HD-R-320-330', http://static1.squarespace.com/static/568f7df70e4c112f75e6c82b/t/571836f84d088ef3a43566fe/1461204731485/Datasheet_PowerXT_Rooftop_320-330_v17_4-18-16.pdf
[7] Patent Application US20150090314 B.N. Yang, Peter P. ; Heng, Jiunn Benjamin ; Reddy, Anand J. ; Xu, Zheng, 2014
[8] Webpage 'SunPower Introduces New Solar Panel: The Performance Series', http://us.sunpower.com/blog/2015/11/12/sunpower-introduces-performance-series-solar-panel/
[9] Press release ' SunEdison inks deal with Solaria to license technology', 2015, http://static1.squarespace.com/static/568f7df70e4c112f75e6c82b/t/56b9b619c6fc081fd55b5d9b/1455011354392/Solaria+SunEd+FINAL_10.26.15.pdf
[10] Ulrich Eitner, Marc Köntges, Rolf Brendel, Measuring thermomechanical displacements of solar cells in laminates using digital image correlation in: 34th IEEE Photovoltaic Specialists Conference, Philadelphia, 2009.
[11] I. Bennett, N. Loiseaux, Measurement of strains in MWT modules during manufacture, Energy Procedia, 27 (2012) 697-702.
[12] Guy Beaucarne, Adriana Zambova, Kees Broek, John Albaugh, Brian Chislea, Jason Wei, Thibault Kervyn de Meerendré, Mario Kloos, Ian Bennett, Durability of silicone electrically conductive adhesive in Metal Wrap-Through module, Energy Procedia, 38 (2013) 482-487.
[13] Guy Beaucarne, Tuukka Savisalo, Henrikki Pantsar, Back-contact MWT modules made with electrically conductive adhesive interconnection and conductive backsheets: study of performance and reliablity through material testing, accelerated aging and field testing, in: European Photovoltaic Solar Energy Conference, Hamburg, Germany, 2015, pp. 1898-1901.